CHEMISTRY
A EUROPEAN JOURNAL

ChemPubSoc
Europe

DOI: 10.1002/chem.201201542

Controlling the Regioselectivity of the Hydrosilylation Reaction in Carbon Nanoreactors

William A. Solomonsz, Graham A. Rance, Mikhail Suyetin, Alessandro La Torre, Elena Bichoutskaia, and Andrei N. Khlobystov*[a]

Abstract: Hollow graphitized carbon nanofibres (GNF) are employed as nanoscale reaction vessels for the hydrosilylation of alkynes. The effects of confinement in GNF on the regioselectivity of addition to triple carbon–carbon bonds are explored. A systematic comparison of the catalytic activities of Rh and RhPt nanoparticles embedded in a nanoreactor with free-standing and surface-adsorbed nanoparticles reveals key mechanisms governing the regioselectivity. Directions of reactions inside GNF are largely controlled by the non-covalent interactions between reactant molecules and the nanofibre channel. The specific π–π interactions increase the local concentration of the aromatic reactant and thus promote the formation of the *E* isomer of the β-addition product. In contrast, the presence of aromatic groups on both reactants (silane and alkyne) reverses the effect of confinement and favours the formation of the *Z* isomer due to enhanced interactions between aromatic groups in the *cis*-orientation with the internal graphitic step-edges of GNF. The importance of π–π interactions is confirmed by studying transformations of aliphatic reactants that show no measurable changes in regioselectivity upon confinement in carbon nanoreactors.

Keywords: carbon · catalysis · nanostructures · nanoreactor · regioselectivity · rhodium

Introduction

Confinement of molecules and atoms inside hollow nanoscale containers provides a powerful strategy for studying structural and chemical properties of individual molecules at the nanoscale.[1–4] Over the past three decades, a variety of nanocontainers, including cyclodextrins, cavitands, calixarenes, cucurbiturils, supramolecular/coordination cages, bilayer vesicles and zeolites,[5,6] have been developed to replicate the behaviour of enzymes in nature and probe the unique way that molecules behave under intense spatial restrictions. In these so-called "nanoreactor" systems, it has been experimentally[7] and theoretically[8] demonstrated that both the kinetics and selectivity of chemical reactions are fundamentally affected by confinement effects; these include altered local concentrations and pressures, preferential alignment of reactants and increased specific non-covalent interactions lowering the activation barriers for reactions relative to the bulk solution or gas phase. As hollow carbon nanostructures, such as carbon nanotubes (CNT) and graphitised nanofibres (GNF), are significantly more thermally stable (up to 700 °C in air and 2800 °C in vacuum) and mechanically more robust (with a tensile strength much higher than that of steel) than any other molecular nanocontainers, the confinement of small molecules[9–11] and other nanoscopic materials[12–13] in CNT has been widely explored. Whereas the surfaces of carbon nanostructures possess rich chemical reactivity,[14] the concave side of the nanotube is relatively chemically unreactive, so that even aggressive chemical processes can be contained within the CNT, which makes hollow carbon nanostructures highly suitable for nanoreactor applications. Indeed, it has been recently shown that composite superstructures comprising metallic species encapsulated in carbon nanotubes exhibit superior activity, chemoselectivity and stereoselectivity as catalysts in chemical transformations, such as the conversion of syngas to ethanol,[15] the Fe_2O_3 catalysed Fischer–Tropsch synthesis[16] and the additive-induced Pt catalysed asymmetric hydrogenation of α-ketoesters.[17] Moreover, the use of carbon nanostructures in catalysis permits examination of two distinct confinement phenomena (Figure 1).

In very narrow containers, such as single-walled carbon nanotubes (SWNT) and small-diameter multi-walled carbon nanotubes (MWNT), encapsulated reactants and catalytic centres are severely confined within the 1D channel (Figure 1 a). The directions and rates of chemical processes in such narrow nanoreactors will differ significantly from those in the bulk phase, thus offering a powerful mechanism for controlling reactions. However, a major drawback of the restricted reaction volume is related to transport resistance in carbon nanostructures.[18,19] As the mean free path of molecules is often larger than the diameter of the carbonaceous nanocontainer, diffusion of molecules in narrow CNT is

[a] W. A. Solomonsz, Dr. G. A. Rance, Dr. M. Suyetin, A. La Torre, Dr. E. Bichoutskaia, Prof. Dr. A. N. Khlobystov
School of Chemistry, University of Nottingham
University Park, Nottingham, NG7 2RD (UK)
Fax: (+44) 115-9513555
E-mail: Andrei.khlobystov@nottingham.ac.uk

Supporting information for this article is available on the WWW under http://dx.doi.org/10.1002/chem.201201542.

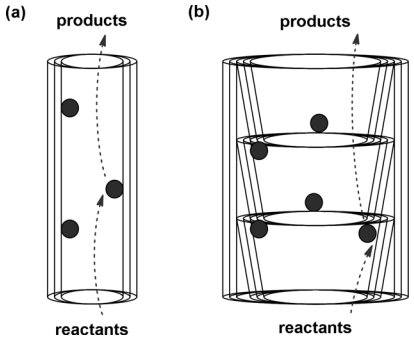

Figure 1. Schematic representation of the two types of carbon nanoreactors: (a) carbon nanotubes (narrow, atomically smooth interior) and (b) graphitised carbon nanofibres (wider, corrugated interior). Circles represent the catalytic centres and arrows indicate the diffusion of reactants in and products out of nanoreactors.

often orders of magnitude lower than in conventional catalysis. Therefore, assessment of the catalyst performance in terms of kinetics is often inappropriate and consequently investigation of mechanisms controlling selectivity of reactions in confined environments can be significantly more valuable.

Graphitised carbon nanofibres have a wider internal volume than CNT, which largely alleviates the problem of transport resistance of reactants/products and ensures that the GNF cavity is always accessible. Whereas GNF are significantly less explored as nanocontainers[12,20] and nanoreactors[12] than CNT, they possess many of the functional characteristics of nanotubes with the added advantage of a larger internal volume. Furthermore, unlike carbon nanotubes, which consist of concentric tubes of graphene, the structures of the inner and outer surfaces of GNF are fundamentally different to each other. The outer surface of GNF consists of continuous, atomically flat cylindrical layers of graphene, but the internal surface possesses a succession of step-edges formed by rolled-up sheets of graphene (3–4 nm high and spaced by 8–15 nm from each other), which act as effective "anchoring points" for molecules and nanoparticles.[21] In general, GNF have the potential to be superior nanoreactors compared with CNT, as their overall tubular topology can create local reaction environments, different to the bulk phase, but without any significant restriction of diffusion, whereas the corrugated internal structure of GNF opens up opportunities to probe local spatial confinement effects in which reactivity and dynamics at the nanofibre–reactant and nanofibre–catalyst interfaces become important.

To explore the effects of a confined environment in carbon nanoreactors on regioselectivity we have chosen the transition-metal-catalysed hydrosilylation of alkynes, which generates vinylsilanes that are particularly useful as synthetic intermediates.[22] The reaction proceeds in the presence of a variety of neutral and cationic metals, such as rhodium,[23] platinum[24] and ruthenium[25,26] and yields a broad distribution of products (Scheme 1).[27,28]

The specific ratio of the Markovnikov α-addition product **1**, the anti-Markovnikov β-addition (*Z* isomer) **2** and the β-addition (*E* isomer) **3** regioisomers and the two dehydrogenative hydrosilylation products (**4** and **5**) is critically dependant on the specific nature of the catalyst and experimental conditions.[29] In this study, we assess the intermolecular hydrosilylation of terminal alkynes using new rhodium-based nanoparticle catalysts located at the internal step-edges of graphitised carbon nanofibres and reveal mechanisms governing the regioselectivity of chemical transformations within carbon nanoreactors.

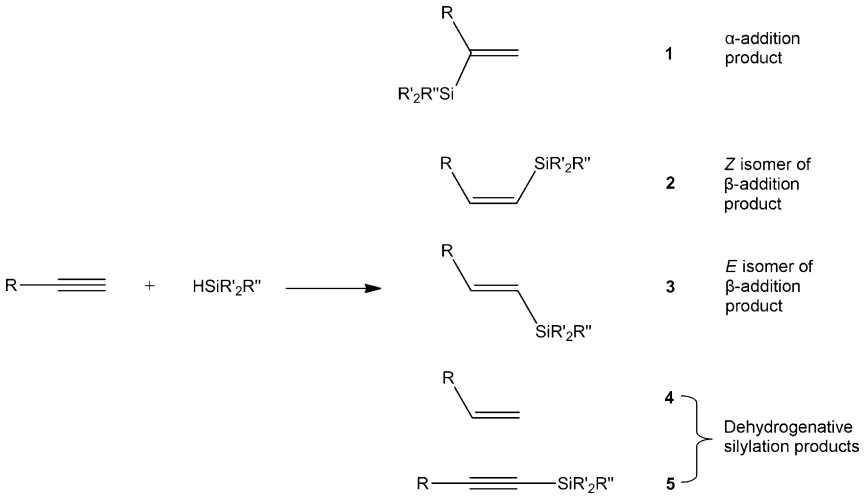

Scheme 1. Generalised reaction scheme for the hydrosilylation of a terminal alkyne yielding a distribution of products: **1** = α-addition, **2** = β-addition (*Z* isomer), **3** = β-addition (*E* isomer), **4** = vinyl product, **5** = alkynylsilane.

Results and Discussion

To assess the effect of nanoscale confinement on the regioselectivity of the hydrosilylation of terminal alkynes, we synthesised a series of novel catalysts using a modification to the approach previously developed within our research group (Scheme 2).[21,30]

The rhodium- (RhNP) and rhodium–platinum (RhPtNP) alloy nanoparticles used in this study were synthesised by adapting the procedure outlined by Murray et al.[31] This versatile preparation has been used to procure large quantities of monodisperse nanoparticles of a variety of metals, including gold,[31] silver,[32] platinum[33] and palladium;[34] in this study we show that the same technique can be successfully applied for rhodium and its intermetallic analogues. To minimise the possible effect of catalyst poisoning, we employed sodium *S*-dodecylthiosulfate (SSDS) as the organic stabiliser

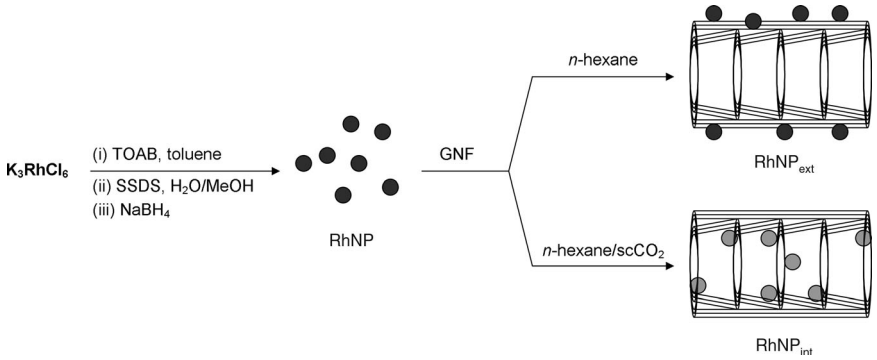

Scheme 2. Schematic representation of the strategy used for the preparation of rhodium nanoparticles and their adsorption on and encapsulation in graphitised carbon nanofibres. An analogous approach was employed for the preparation of the rhodium–platinum nanoparticulate system.

in our nanoparticle synthesis because it has been recently shown by Shon et al.[35] that similar palladium nanoparticles possessed superior catalytic ability relative to those prepared using more conventional dodecanethiol, due to a reduction in the surface coverage of ligand. This resulted in fewer metal–sulphur bonds that poison the surface of the nanoparticle and allowed more efficient adsorption of organic substrates, features that are critical for efficient catalysis.[36] Identical, low quantities of the as-prepared nanoparticles were then supported on the external surface ($RhNP_{ext}$) and confined in the inner cavity ($RhNP_{int}$) of graphitised carbon nanofibres using conventional organic solvents and a mixture of hexane/carbon dioxide under supercritical conditions respectively and the resultant materials characterised by a range of complementary techniques (Figure 2 and S2–S4 in the Supporting Information). A typical loading of the metal catalyst was estimated to be 5–6 and 3–4 weight% for the $RhNP_{ext}$/$RhNP_{int}$ and $RhPtNP_{ext}$/$RhPtNP_{int}$ samples, respectively. Systematic comparison of the catalytic activities of these systems enables discrimination between the possible effects of catalyst support and confinement.

As nanoparticle-catalysed reactions are potentially sensitive to composition (e.g., size, shape and surfactant surface density) of the catalyst, it was important to establish that these attributes were unaffected by the assembly procedures and as can be seen from the micrographs (Figure S4.1 in the Supporting Information) all nanoparticles were roughly spherical in morphology and around 3 nm in mean diameter (2.9 ± 0.4, 2.7 ± 0.4 and 2.9 ± 0.3 nm for RhNP, $RhNP_{ext}$ and $RhNP_{int}$, respectively). Due to the similar contrast of the RhNP and the GNF walls it is difficult to definitively describe the location and density of the nanoparticles in the composite materials; however, it was found that in excess of 80% of RhNP are adsorbed on the exterior surface in $RhNP_{ext}$ and more than 85% of RhNP are confined within nanofibres in $RhNP_{int}$.

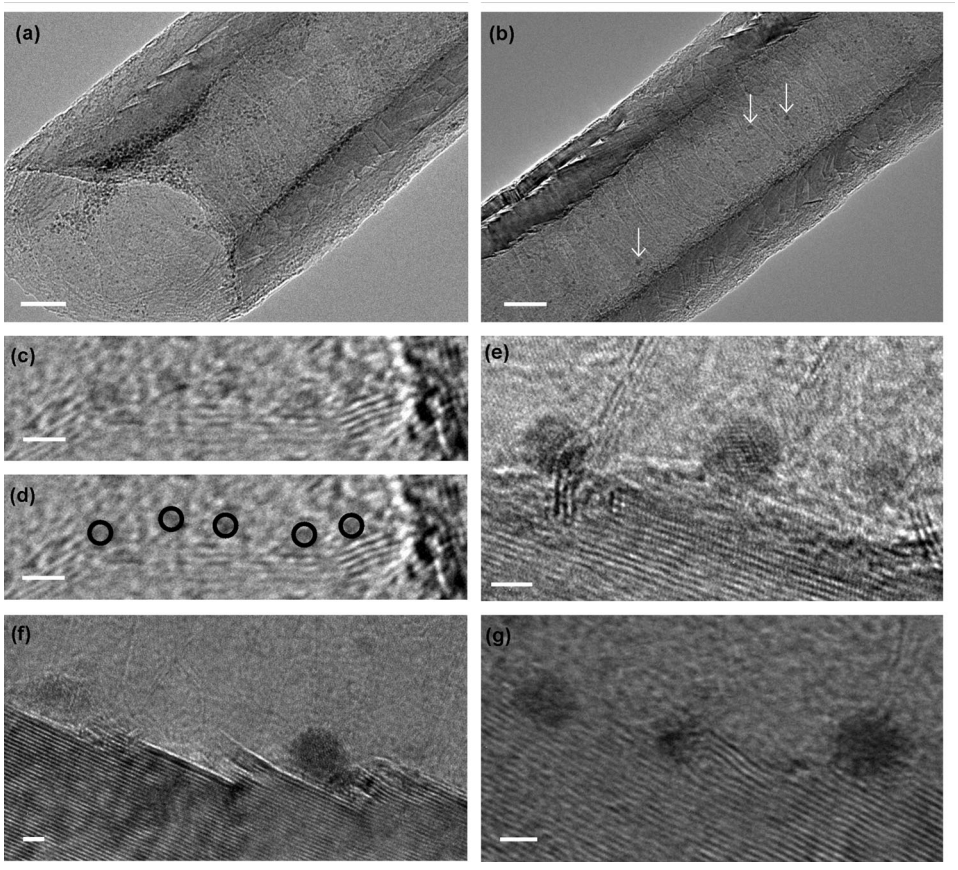

Figure 2. Bright-field transmission electron micrographs of the GNF nanoreactors. Image (a) shows the open-end of a nanoreactor, where an array of RhNP resides at the internal step-edges. A section from the middle of the nanoreactor is shown in (b) in which the rhodium nanoparticles appear as dark circles (three examples of RhNP are highlighted by white arrows). Image (c) shows a high-magnification area of the step-edge of a nanoreactor, although due to the low atomic weight of rhodium and thickness of GNF, nanoparticles are difficult to distinguish at the step-edges; the black circles in (d) highlight the positions of the RhNP. By using thermal annealing to increase the size of RhNP it was possible to ascertain their positions at the GNF step-edges, as shown in (e–g). Scale bars are 20 nm (a)–(b) and 2 nm (c)–(g) (see Figure S4.2 in the Supporting Information for micrographs of the corresponding RhPtNP analogues).

Furthermore, it is significant to note that encapsulated nanoparticles seemingly reside at the internal step-edges of the nanofibre, due to increased van der Waals interactions between the RhNP and the graphitic surface of the GNF interior[20] and therefore the commensurate size of the RhNP and the step-edge (Figure 2) permits us to investigate the effect of local spatial confinement on chemical reactions.

The rhodium-catalysed hydrosilylation of phenylacetylene using triethylsilane has been investigated by a number of research groups and has been shown to proceed highly unselectively yielding all five possible products, each of which is readily identifiable by ^{1}H NMR spectroscopy and GC-MS (Figure 3).[24,26]

The ^{1}H NMR spectra of products **1–4** have unique and distinguishable shifts and multiplicities in the region of $\delta_H =$ 5–7 ppm due to the presence of vinylic protons. Both of the doublets corresponding to the α product (**1**) appear in this region, although only one pair of the β-(*Z*) (**2**) and β-(*E*) (**3**) doublets may be seen because their counterparts appear in the crowded aromatic region beyond $\delta_H = 7$ ppm. As **5** has no vinylic protons that allow diagnosis in this way using ^{1}H NMR spectroscopy, the presence of this compound (and all others) was confirmed by GC-MS.

Following optimisation of the reaction conditions, in which it was observed that elevated temperatures (90 °C) were necessary to overcome the tardy reaction kinetics associated with the necessary extremely low loading of catalyst employed in the reaction, all new catalytic materials were tested in the hydrosilylation of a series of alkynes and the effect of confinement assessed (Table 1; see also Table S6 in the Supporting Information). It is important to note that our control experiments with catalytic nanoparticles adsorbed on the outer surface of GNF ($RhNP_{ext}$ and $RhPtNP_{ext}$) exhibit regioselectivity intermediate between free-standing and confined catalysts. To emphasise the effects of spatial confinement within nanofibres, the selectivity of different reactions carried out in GNF is calibrated to that on GNF surface.

Table 1. The effect of confinement in GNF with respect to the supported catalysts. For full quantitative analysis please see Table S6 in Supporting Information.

Catalyst	R	R′	R″	Regioselectivity[a]	
				Change in the *Z*/*E* isomeric ratio	Change in the amount of **4** and **5**
RhNP	Ph	Et	Et	5.8-fold decrease	3.0-fold increase
RhPtNP	Ph	Et	Et	no change	1.6-fold increase
RhNP	Ph	Me	Ph	2.6-fold increase	no change
RhNP	Cy	Et	Et	no change	no change
RhNP	*n*-Oct	Et	Et	no change	no change

[a] If comparative values were within the determined 3% experimental error, we concluded that no change was apparent.

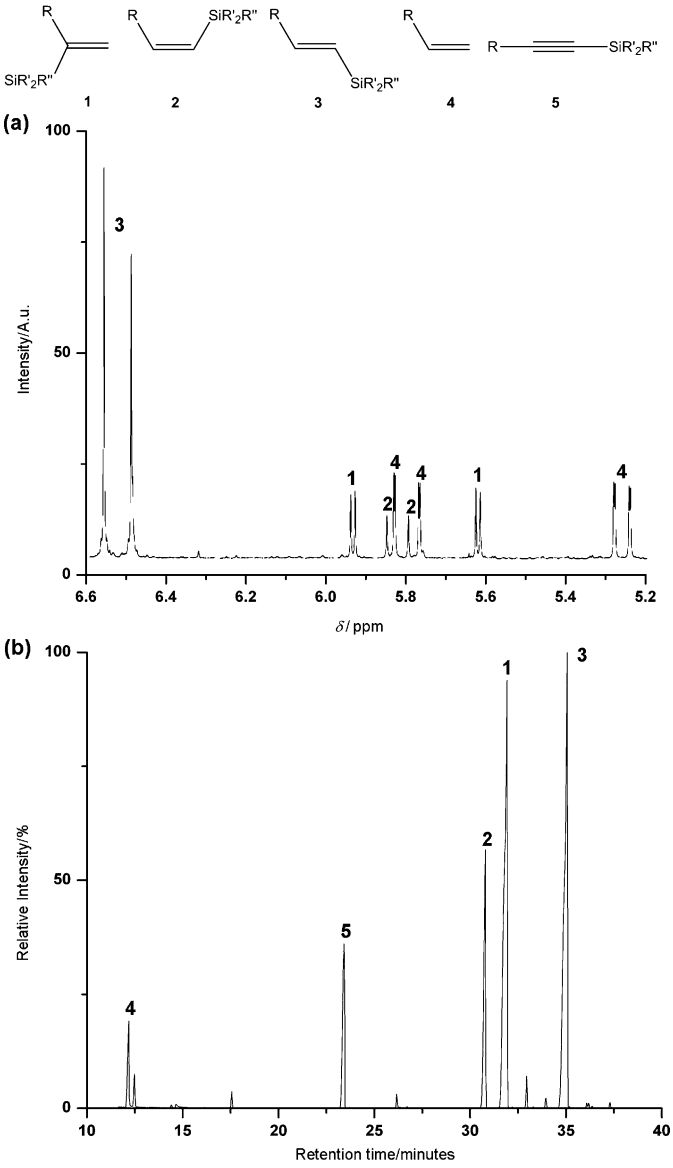

Figure 3. Comparative techniques used to evaluate the distribution of products in the hydrosilylation of phenylacetylene using triethylsilane: (a) quantitative ^{1}H NMR spectroscopy consistent with known literature values (b) qualitative GC-MS (the corresponding mass spectra are shown in Figure S5 in the Supporting Information).

Our observations clearly indicate that the regioselectivity of the hydrosilylation reaction is significantly affected by spatial confinement in carbon nanoreactors. Inside GNF, the yield of the β-(*E*) (**3**) product of the triethylsilane addition to phenylacetylene increases by a factor of 5.8 as compared with its geometric isomer β-(*Z*) (**2**) and a greater than 10-fold increase in selectivity of this product inside nanoreactors as compared with the bulk solution phase (Table S6 in the Supporting Information). Confinement in nanoreactors also promotes a 3.0-fold increase in products of dehydrogenative silylation (Table 1). A similar trend was observed for a different catalytic system, RhPtNP, whereby confinement of the catalyst also resulted in a promotion of the dehydrogenative silylation products. However, this effect was less pronounced as the presence of Pt measurably enhances the selectivity of this reaction even without confinement (Table S6

in the Supporting Information), as expected for catalysis by platinum.[37]

This apparent enhanced regioselectivity inside nanoreactors was an astonishing and unexpected result. However, to confirm that the observed trends were related to confinement of the catalyst numerous control experiments were conducted (see S7 in the Supporting Information). As this reaction is so sensitive to the nature of the catalyst,[29] a number of compositional parameters of the metallic nanoparticles were varied in an attempt to account for the above findings. From these control experiments, it was confirmed that nanoparticle size, loading and density of the capping ligand do not significantly affect the product distribution in such a way that would account for the observations made. Furthermore, experimental conditions, such as temperature in the range of 75–105 °C relevant to our studies, have minimal effect on the product distribution. It is significant to note, however, that changes in the stoichiometry of reactants had a noticeable effect on the regioselectivity (Table S7.5 in the Supporting Information), hence a 1:1 molar ratio of the starting alkyne and silane were strictly maintained in all experiments comparing the regioselectivity of hydrosilylation.

Supramolecular interactions of reactant molecules with nanoreactors are often responsible for the altered reactivity observed in confined reactions.[6] Considering the graphitic nature of nanofibres, phenylacetylene is expected to have a higher affinity for GNF than triethylsilane due to specific π–π interactions between the former reactant and the GNF. In this context, we define π–π interactions as the dispersion forces between the quadrupole moment of the small aromatic molecule with the highly polarisable and delocalised π-system of the carbon nanofibre.[38] This would lead to a higher local concentration of the acetylene bearing the aromatic phenyl group within the nanoreactor which can affect the course of the reaction. Control measurements with free-standing RhNP carried out for different alkyne/silane molar ratios, clearly demonstrate that increased concentration of alkyne favours the formation of dehydrogenative silylation products at the expense of the β-(*Z*) isomer (Table S7.5 in the Supporting Information). This result is consistent with the observed changes of regioselectivity inside GNF (Table 1), confirming that confinement increases the local concentration of alkyne.

To test this mechanism, additional control experiments using cyclohexylacetylene or 1-decyne as the alkynyl component were conducted (Table 1 and Table S5 in the Supporting Information) which showed no changes in regioselectivity upon spatial confinement in nanofibres for the reactions of molecules without aromatic moieties. Aromatic interactions of the reactants with the nanofibre interior leading to higher local concentrations is an important factor in such reactions, particularly because steric arguments cannot explain the difference in the behaviours of phenylacetylene and cyclohexylacetylene that have comparable sizes and shapes.

When both reactants (acetylene and silane) possess aromatic groups a trend qualitatively different to the hydrosilylation using trialkylsilane was observed. The main effect of the introduction of a phenyl group in the silane reactant (e.g., $HSiMe_2Ph$) is that upon confinement in GNF the regioselectivity of addition changes in the opposite direction to trialkylsilanes (e.g., $HSiEt_3$). Indeed, when using a RhNP nanoreactor, the formation of the β-(*Z*) product (**2**) becomes more favourable for the addition of $HSiMe_2Ph$ to phenylacetylene, at the expense of the β-(*E*) and no promotion of the dehydrogenative silylation products is observed (Table 1). These observations can be rationalised on the basis of mechanistic considerations (Scheme 3).

A number of previous literature reports have described the mechanism for the formation of specific products within the catalytic cycle,[24] however, a comprehensive mechanism accounting for all five of the products observed in our experiments has yet to be established. The scheme we propose combines known mechanistic concepts and is based primarily on a modified Chalk–Harrod cycle (also referred to as the Crabtree–Ojima cycle) in which silylmetallation in the initial step leads to a mixture of products (Scheme 3). The key step in the mechanism appears to be when intermediate **A** either relieves steric repulsion between the metal-containing group and the silyl R′/R″ groups to form intermediate **B**, or transforms into the thermodynamically most stable β-(*E*) product (**3**). Intermediate **B** can also undergo metal hydride β-elimination, which subsequently leads to the formation of the dehydrogenative silylation products (Scheme 3).

The experimental data shows that the percentage of products formed from intermediate **B** (**1**, **2**, **4** and **5**) relative to intermediate **A** remains constant when R = Ph and R′ = R″ = Et, which is indicative of no change in the relative stabilities of these intermediates upon confinement in GNF. However, the relative distribution of products formed from **B** is significantly affected by confinement (a 17-fold and a 4-fold decrease in the β-(*Z*):**4**+**5** ratio was observed using RhNP and RhPtNP in GNF, respectively). This implies that metal hydride β-elimination to produce **4** and **5** is favoured over the formation of **2**, commensurate with a higher local concentration of phenylacetylene. However, as the interconversion between **A** and **B** is a reversible process, bulky R and R′ groups may destabilise **B** in favour of intermediate **A** thus enhancing the yield of the thermodynamically most stable *E* isomer of the β-addition product.[28] It is, therefore, a remarkable result that when R = Ph and R′ = Me, R″ = Ph, the less stable *Z* isomer (**2**) is actually favoured inside a GNF. In this case, the percentage of products formed from intermediate **B** (**1**, **2**, **4** and **5**) as compared with intermediate **A** increases, indicative of a difference in the relative stabilities of **A** and **B** and accounts for the regioselective switching inside GNF. Hence, the effects of local concentration, expected to be significant in this system as both substrates bear aromatic moieties, are negated, that is, no promotion of products **4** and **5** upon encapsulation was observed and the relative stabilities of intermediates must be responsible.

To probe this further, the calculated total energies of the optimised geometries of **A** and **B** when R = Ph, R′ = Me and

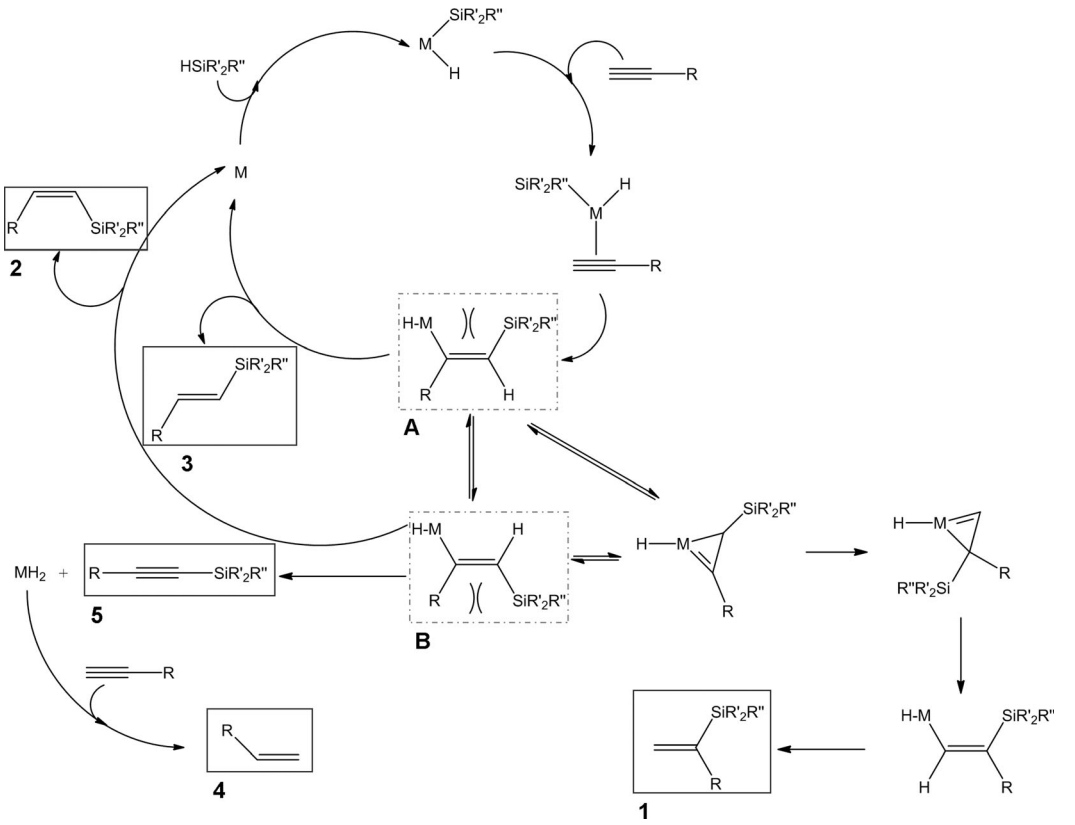

Scheme 3. The mechanism of the hydrosilylation reaction. Isolatable reaction products (**1**–**5**) and key reaction intermediates (**A** and **B**) are highlighted by solid- and dashed-line boxes, respectively.

R″ = Ph were compared. Our density functional theory (DFT) calculations of the relative geometries and energetics of the two intermediates under standard conditions assist in our explanation of experimental observations, showing that intermediate **A** is more stable than **B** (by ca. 1 eV), which is consistent with the fact that intermediate **A** generates the thermodynamically more favourable *E* isomer. However, the geometries of these structures are very different: **B** is splayed with the two phenyl rings lying co-planar to each other at opposite ends of the molecule, whereas **A** adopts a pearl-shell like structure with the two aromatic moieties encompassing the rhodium catalyst (Figure 4). Depending on the specific nature and consequent steric bulk of the active catalyst, which could be either a low coordination rhodium atom at the vertex of the nanoparticle surface or a leached species formed during catalysis,[39] the geometry of **B** in the real system may be slightly more splayed. Irrespective of the degree of splaying, it is evident that attractive interactions between each of the intermediates and the underlying graphitic surface of the nanoreactor step-edge are greater for **B** than **A**, as the more open shape of **B** results in a larger area of surface contact with the GNF step-edge.

Thus, the orientation of the phenyl groups in the case of the β-(*Z*) isomer and its precursor intermediate **B** facilitates maximal attractive π–π interactions with the graphitic step-edge. When both reactants carry aromatic groups, the local nanoscale morphology of the inner surface of GNF step

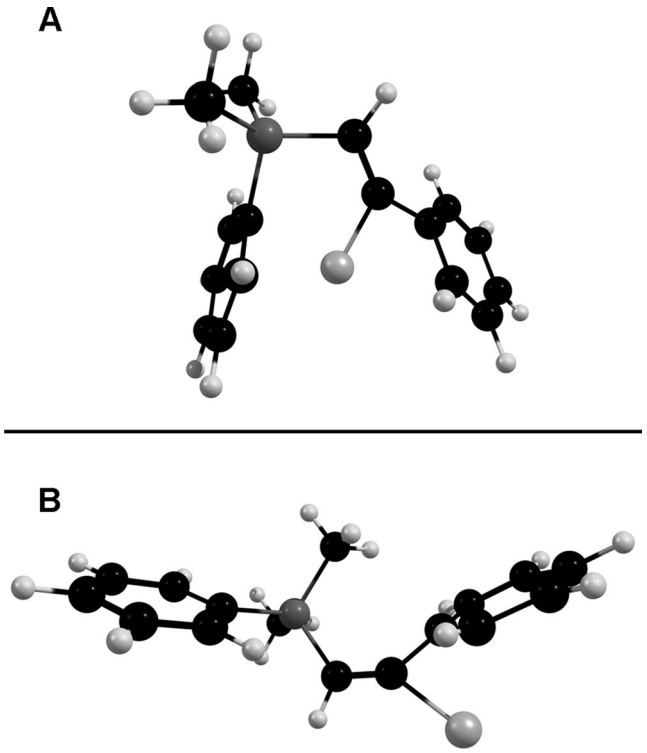

Figure 4. DFT optimised geometries of intermediates **A** (top) and **B** (bottom).

edges mitigates the steric repulsion between R on the alkyne and R′/R″ on the silane and promotes the formation of the thermodynamically less stable isomer. Furthermore, this implies that enhanced specific interactions between the reactants and the nanofibre at the nanoparticle–nanofibre interface play a role as significant as the increased local concentrations of reactants for reactions in a carbon nanocontainer.

Conclusion

We report the first observation of regioselectivity switching of a preparative chemical reaction due to spatial confinement in carbon nanostructures. The precise structures of reactant molecules crucially determine the effects of confinement, with the balance of aliphatic and aromatic moieties being the most important parameter. Depending on the nature of reactants, three main trends are observed in carbon nanoreactors: 1) when neither alkyne nor silane bears aromatic moieties, no favourable attractive interactions exist with the interior of nanoreactor and therefore no confinement effect is observed; 2) when only the alkyne is aromatic, a characteristic increase in the amount of dehydrogenative silylation products and decrease in the β-(*Z*): β-(*E*) isomers ratio is observed, which is related to the increased local concentration of the aromatic reactant (phenylacetylene) within the GNF cavity; 3) when both alkyne and silane possess aromatic groups, maximised aromatic stacking interactions between phenyl groups on the reactive intermediates and the nanofibre at the nanoparticle-nanofibre interface are sufficient to overcome the effects of local concentrations and favour the formation of the thermodynamically less stable β-(*Z*) regioisomer.

As the understanding of the physicochemical properties of carbon nanostructures as nanoscale containers and substrates under a variety of different conditions, including those relevant to biological systems,[40,41] is advancing rapidly, carbon cavities become increasingly important for controlling the structure and reactivity of encapsulated molecules. Our approach for catalyst assembly and experimental methodology for monitoring the selectivity of reactions in carbon nanostructures are general and applicable for a wide variety of chemical transformations. In this study we have established mechanisms for controlling the regioselectivity of reactions in confinement which will guide further development towards the preparative applications of carbon nanoreactors.

Experimental Section

General procedures: All reagents and solvents were purchased from Sigma–Aldrich, UK and used without further purification. Water was purified (>18 MΩ cm) using a Barnstead NANOPure II system and toluene was distilled over calcium hydride. The PR24 GNF were purchased from Applied Science, USA and produced via chemical vapour deposition. All glassware was cleaned with a mixture of hydrochloric and nitric acid (3:1 v/v, "aqua regia") and rinsed thoroughly with deionised water, cleaned with potassium hydroxide in isopropyl alcohol and finally rinsed thoroughly with deionised water before use. ^{1}H NMR spectra were obtained using a Bruker DPX-300 (300.13 MHz) spectrometer at 298 K using $CDCl_3$ as the solvent. Integration was carried out to quantify the product distribution based on the most upfield 1-proton doublet(s). The overall distribution of products was then quantified by calculating the integral value for a product as a percentage figure of the sum of all integrals. GC-MS was performed using a VG Autospec in EI$^+$ mode. Thermogravimetric analysis was performed using a TA Instruments SDT Q600 under a flow of oxygen at a rate of 100 mL min^{-1} at a heating rate of 10 °C min^{-1} from room temperature to 900 °C. Transmission electron microscopy was performed using a JEOL 2100F TEM (field emission gun source, information limit <0.19 nm) at room temperature. Samples were typically prepared by drop-drying onto a copper grid mounted "holey" or continuous carbon films. Average particle diameters (d_{NP}) were calculated on the basis of counting at least 100 particles from different micrographs, using Gatan Digital Micrograph software and ImageJ. UV/Vis spectra were recorded in toluene using 1 cm quartz cells on a Perkin–Elmer Lambda 25 UV/Vis spectrophotometer at a scan rate of 480 nm min^{-1} over the range 190–1100 nm. IR spectra were measured in the solid state using a Bruker Tenser 27 ATR FT-IR spectrometer over the range 400–4000 cm^{-1}. All filtrations were carried out using Whatman 0.2 μm polytetrafluoroethylene (PTFE) membranes. Where high pressure techniques were required, all equipment was leak-tested immediately prior to use.

Catalyst preparation: The preparation of rhodium and rhodium-platinum alloy nanoparticles is based on a modified two-phase Brust–Schiffrin reduction.[42] A typical synthesis for the preparation of rhodium nanoparticles is described as follows: to a stirred solution of potassium hexachlororhodate (157 mg, 0.36 mmol, 2.7 equiv) in deionised water (12.5 mL) was added a separate solution containing tetraoctylammonium bromide (550 mg, 1.0 mmol, 7.5 equiv) in toluene (25 mL) and the resultant biphasic mixture was vigorously stirred for 10 min at room temperature. The phases were separated, the aqueous phase discarded and to the remaining organic phase was added tetraoctylammonium bromide (550 mg, 1.0 mmmol, 7.5 equiv) and a separate solution of sodium *S*-dodecylthiosulfate (40 mg, 0.13 mmol, 1 equiv) in water/methanol (10 mL, 3:1 v/v) and the mixture stirred for 10 min at room temperature. To this was added a separate solution containing sodium borohydride (150 mg, 5 mmol, 37.5 equiv) in deionised water (7.5 mL) and the combined mixture vigorously stirred for 16 h at room temperature. The phases were separated, the aqueous phase discarded and the organic phase retained, washed with deionised water (3×100 mL), dried over anhydrous magnesium sulphate, filtered and the solvent removed concentrated in vacuo. To this was added ethanol (900 mL) and the product precipitated at −30 °C over 16 h, collected by vacuum filtration (0.20 μm, PTFE), washed with ethanol (300 mL) and acetone (300 mL) and dried in vacuo to yield a dark solid (17.2 mg). The as-prepared nanoparticles were supported on pristine nanofibres at room temperature under ultrasonication[30] and confined within the same nanofibres using a mixture of hexane/CO_2 under supercritical conditions[13] (see S1–S3 in the Supporting Information).

Hydrosilylation of terminal alkynes with hydrosilanes: The catalyst (0.30 mg and 0.15 mg metal content for RhNP and RhPtNP systems, respectively) and the hydrosilane (18 mmol) were added to an argon-flushed Schlenk tube. The alkyne (18 mmol) was then added dropwise. The mixture was homogenised with brief ultrasonication at room temperature and stirred at the required reaction temperature of 90 °C. The progress of the reaction was monitored primarily by ^{1}H NMR spectroscopy, taking aliquots (0.25 mL) of the mixture at regular intervals to provide quantitative analysis of reaction progress and product distribution. GC-MS was used for qualitative analysis of the composition of the crude mixture.

Molecular modelling: The geometry optimisations of the molecules have been obtained with the DFT/B3LYP level of theory and the Grimme empirical dispersion corrections[43] as implemented in the Q-Chem quantum chemistry package.[44] The effective core potential LANL2DZ basis set has been used for the rhodium atom, and the 6–31G* basis set for all other atoms.

Acknowledgements

The authors thank the European Science Foundation, the European Research Council, the Royal Society and the University of Nottingham for supporting this research, the Nottingham Nanoscience and Nanotechnology Centre for access to TEM facilities and Dr. Mick Cooper for his analytical services. E.B. acknowledges the Engineering and Physical Sciences Research Council (EPSRC) for funding a Career Acceleration Fellowship EP/G005060/1.

[1] A. N. Khlobystov, *ACS Nano* **2011**, *5*, 9306–9312.
[2] P. Serp, E. Castillejos, *ChemCatChem* **2010**, *2*, 41–47.
[3] X. Pan, X. Bao, *Acc. Chem. Res.* **2011**, *44*, 553–562.
[4] D. A. Britz, A. N. Khlobystov, *Chem. Soc. Rev.* **2006**, *35*, 637–659.
[5] G. Borsato, J. Rebek Jr., A. Scarso, in *Selective Nanocatalysts and Nanoscience* (Eds.: A. Zecchina, S. Bordiga, E. Groppo), Wiley-VCH, Weinheim, **2011**, pp. 105–108.
[6] *Molecular Encapsulation: Organic Reactions in Constrained Systems* (Eds.: U. H. Brinker, J.-L. Mieusset), Wiley, New York, **2010**.
[7] C. Christensen, K. Johannsen, I. Schmidt, *J. Am. Chem. Soc.* **2003**, *125*, 13370–13371.
[8] E. Santiso, M. Kostov, A. George, M. Buongiorno, K. Gubbins, *Appl. Surf. Sci.* **2007**, *253*, 5570–5579.
[9] S. Ittisanronnachai, H. Orikasa, N. Inokuma, Y. Uozu, T. Kyotani, *Carbon* **2008**, *46*, 1361–1363.
[10] K. Schulte, J. Swarbrick, N. Smith, F. Bondino, E. Magnano, A. N. Khlobystov, *Adv. Mater.* **2007**, *19*, 3312–3316.
[11] D. Tománek, *Phys. B* **2002**, *323*, 86–89.
[12] E. Castillejos, P.-J. Debouttiere, L. Roiban, A. Solhy, V. Martinez, Y. Kihn, O. Ersen, K. Philippot, B. Chaudret, P. Serp, *Angew. Chem.* **2009**, *121*, 2567–2571; *Angew. Chem. Int. Ed.* **2009**, *48*, 2529–2533.
[13] E. Castillejos, R. Chico, R. Bacsa, S. Coco, P. Espinet, M. Perez-Cadenas, A. Guerrero-Ruiz, I. Rodriguez-Ramos, P. Serp, *Eur. J. Inorg. Chem.* **2010**, 5096–5102.
[14] S. A. Hodge, M. K. Bayazit, K. S. Coleman, M. S. P. Shaffer, *Chem. Soc. Rev.* **2012**, *41*, 4409–4429.
[15] X. Pan, Z. Fan, W. Chen, Y. Ding, H. Luo, X. Bao, *Nat. Mater.* **2007**, *6*, 507–511.
[16] W. Chen, Z. Fan, X. Pan, X. Bao, *J. Am. Chem. Soc.* **2008**, *130*, 9414–9419.
[17] Z. Chen, Z. Guan, M. Li, Q. Yang, C. Li, *Angew. Chem.* **2011**, *123*, 5015–5019.
[18] S. Xu, W. Zhang, X. Liu, X. Han, X. Bao, *J. Am. Chem. Soc.* **2009**, *131*, 13722–13727.
[19] D. A. Newsome, D. S. Sholl, *Nano Lett.* **2006**, *6*, 2150–2153.
[20] A. La Torre, M. C. Gimenez-Lopez, M. Fay, G. A. Rance, W. A. Solomonsz, T. W. Chamberlain, P. D. Brown, A. N. Khlobystov, *ACS Nano* **2012**, *6*, 2000–2007.
[21] A. La Torre, M. Fay, G. A. Rance, M. C. Gimenez-Lopez, W. A. Solomonsz, P. D. Brown, A. N. Khlobystov, *Small* **2012**, *8*, 1222–1228.
[22] I. Fleming, J. Dunogues, R. Smithers, *Org. React.* **1989**, *37*, 57–575.
[23] Y. Goldberg, H. Alper, *Tetrahedron Lett.* **1995**, *36*, 369–372.
[24] L. Lewis, K. Sy, G. Bryant, P. Donahue, *Organometallics* **1991**, *10*, 3750–3759.
[25] M. Jiménez, J. Pérez-Torrente, M. Bartolomé, V. Gierz, F. Lahoz, L. Oro, *Organometallics* **2008**, *27*, 224–234.
[26] H. Katayama, K. Taniguchi, M. Kobayashi, T. Sagawa, T. Minami, F. Ozawa, *J. Organomet. Chem.* **2002**, *645*, 192–200.
[27] C.-H. Jun, R. Crabtree, *J. Organomet. Chem.* **1993**, *447*, 177–187.
[28] B. Marciniec, H. Maciejewski, C. Pietraszuk, P. Pawluć, in *Hydrosilylation: A Comprehensive Review on Recent Advances, Vol. 1* (Ed.: B. Marciniec), Springer, London, **2009**, pp. 53–72.
[29] R. Takeuchi, N. Tanouchi, *J. Chem. Soc. Perkin Trans. 1* **1994**, 2909–2913.
[30] G. A. Rance, D. H. Marsh, S. J. Bourne, T. J. Reade, A. N. Khlobystov, *ACS Nano* **2010**, *4*, 4920–4928.
[31] Y.-S. Shon, S. Gross, B. Dawson, M. Porter, R. Murray, *Langmuir* **2000**, *16*, 6555–6561.
[32] Y.-S. Shon, E. Cutler, *Langmuir* **2004**, *20*, 6626–6630.
[33] E. G. Castro, R. V. Salvatierra, W. H. Schreiner, M. M. Oliveira, A. J. G. Zarbin, *Chem. Mater.* **2010**, *22*, 360–370.
[34] F. Zamborini, S. Gross, R. Murray, *Langmuir* **2001**, *17*, 481–488.
[35] E. Sadeghmoghaddam, C. Lam, D. Choi, Y.-S. Shon, *J. Mater. Chem.* **2011**, *21*, 307–312.
[36] B. Chauhan, J. Rathore, T. Bandoo, *J. Am. Chem. Soc.* **2004**, *126*, 8493–8500.
[37] J. Speier, *Adv. Organomet. Chem.* **1979**, *17*, 407–447.
[38] C. R. Martinez, B. L. Iverson, *Chem. Sci.* **2012**, *3*, 2191–2201.
[39] M. T. Reetz, J. G. de Vries, *Chem. Commun.* **2004**, 1559–1563.
[40] Z. Hu, G. D. Pantos, N. Kuganathan, R. L. Arrowsmith, R. M. J. Jacobs, G. Kociok-Köhn, J. O'Byrne, K. Jurkschat, P. Burgos, R. M. Tyrrell, S. W. Botchway, J. K. M. Sanders, S. I. Pascu, *Adv. Funct. Mater.* **2012**, *22*, 503–518.
[41] A. Di Crescenzo, D. Velluto, J. A. Hubbell, A. Fontana, *Nanoscale* **2011**, *3*, 925–938.
[42] M. Brust, M. Walker, D. Bethell, D. Schiffrin, R. Whyman, *J. Chem. Soc. Chem. Commun.* **1994**, 801–802.
[43] S. Grimme, *J. Comput. Chem.* **2006**, *27*, 1787–1799.
[44] Y. Shao, L. Fusti-Molnar, Y. Jung, J. Kussmann, C. Ochsenfeld, S. T. Brown, A. T. B. Gilbert, L. V. Slipchenko, S. V. Levchenko, D. P. O'Neill, R. A. DiStasio Jr., R. C. Lochan, T. Wang, G. J. O. Beran, N. A. Besley, J. M. Herbert, C. Y. Lin, T. Van Voorhis, S. H. Chien, A. Sodt, R. P. Steele, V. A. Rassolov, P. E. Maslen, P. P. Korambath, R. D. Adamson, B. Austin, J. Baker, E. F. C. Byrd, H. Daschel, R. J. Doerksen, A. Dreuw, B. D. Dunietz, A. D. Dutoi, T. R. Furlani, S. R. Gwaltney, A. Heyden, S. Hirata, C.-P. Hsu, G. Kedziora, R. Z. Khaliullin, P. Klunzinger, A. M. Lee, M. S. Lee, W. Z. Liang, I. Lotan, N. Nair, B. Peters, E. I. Proynov, P. A. Pieniazek, Y. M. Rhee, J. Ritchie, E. Rosta, C. D. Sherrill, A. C. Simmonett, J. E. Subotnik, H. L. Woodcock III, W. Zhang, A. T. Bell, A. K. Chakraborty, D. M. Chipman, F. J. Keil, A. Warshel, W. J. Hehre, H. F. Schaefer III, J. Kong, A. I. Krylov, P. M. W. Gill, M. Head-Gordon, *Phys. Chem. Chem. Phys.* **2006**, *8*, 3172–3191.

Received: May 3, 2012
Published online: September 11, 2012

